Tunable two-dimensional electron gas at the interfaces of ferroelectric potassium tantalate niobates

Jia-Xin Lv(吕嘉信), Si-Lan Li(李思澜), Chen-Hao Duan(段辰昊), Shuan-Hu Wang(王拴虎), Hong Yan(闫虹), Ke-Xin Jin(金克新)

Citation: Chin. Phys. B. 35, 107302 (2026). DOI: 10.1088/1674-1056/ae5475 | CSTR: 32038.14.CPB.ae5475
http://cpb.iphy.ac.cn; http://iopscience.iop.org/cpb

What follows is a list of articles you may be interested in

Role of self-assembled molecules' anchoring groups for surface defect passivation and dipole modulation in inverted perovskite solar cells

Xiaoyu Wang(王啸宇), Muhammad Faizan, Kun Zhou(周琨), Xinjiang Wang(王新江), Yuhao Fu(付钰豪), Lijun Zhang(张立军)

Chin. Phys. B. 33, 107303 (2024). DOI: 10.1088/1674-1056/ad711f

Low-damage interface enhancement-mode AlN/GaN high electron mobility transistors with 41.6% PAE at 30 GHz

Si-Yu Liu(刘思雨), Jie-Jie Zhu(祝杰杰), Jing-Shu Guo(郭静姝), Kai Cheng(程凯), Min-Han Mi(宓珉瀚), Ling-Jie Qin(秦灵洁), Bo-Wen Zhang(张博文), Min Tang(唐旻), Xiao-Hua Ma(马晓华)

Chin. Phys. B. 32, 117302 (2023). DOI: 10.1088/1674-1056/acd8a5

Impact of low-dose radiation on nitrided lateral 4H-SiC MOSFETs and the related mechanisms

Wen-Hao Zhang(张文浩), Ma-Guang Zhu(朱马光), Kang-Hua Yu(余康华), Cheng-Zhan Li(李诚瞻), Jun Wang(王俊), Li Xiang(向立), Yu-Wei Wang(王雨薇)

Chin. Phys. B. 32, 057305 (2023). DOI: 10.1088/1674-1056/acbd2e

Superconductivity in epitaxially grown $LaVO_3/KTaO_3(111)$ heterostructures

Yuan Liu(刘源), Zhongran Liu(刘中然), Meng Zhang(张蒙), Yanqiu Sun(孙艳秋), He Tian(田鹤), Yanwu Xie(谢燕武)

Chin. Phys. B. 32, 037305 (2023). DOI: 10.1088/1674-1056/acac1b

Ozone oxidation of 4H-SiC and flat-band voltage stability of SiC MOS capacitors

Zhi-Peng Yin(尹志鹏), Sheng-Sheng Wei(尉升升), Jiao Bai(白娇), Wei-Wei Xie(谢威威), Zhao-Hui Liu(刘兆慧), Fu-Wen Qin(秦福文), De-Jun Wang(王德君)

Chin. Phys. B. 31, 117302 (2022). DOI: 10.1088/1674-1056/ac7ccf

---

Tunable two-dimensional electron gas at the interfaces of ferroelectric potassium tantalate niobates

Jia-Xin Lv(吕嘉信), Si-Lan Li(李思澜), Chen-Hao Duan(段辰昊), Shuan-Hu Wang(王拴虎), Hong Yan(闫虹), and Ke-Xin Jin(金克新)†

Shaanxi Key Laboratory of Condensed Matter Structures and Properties and MOE Key Laboratory of Materials Physics and Chemistry under Extraordinary Conditions, School of Physical Science and Technology, Northwestern Polytechnical University, Xi'an 710072, *China*

(Received 10 December 2025; revised manuscript received 2 March 2026; accepted manuscript online 19 March 2026)

Heterointerfaces in complex oxides have emerged as a promising platform for exploring novel physical phenomena and advancing integrated technologies in sensing, storage, and computing. However, achieving precise control over a two-dimensional electron gas (2DEG) in ferroelectric oxide-based field-effect transistors (FETs) remains a significant challenge. In this study, we report a tunable 2DEG system realized by depositing an amorphous $LaAlO_3$ layer onto a (001)-oriented ferroelectric potassium tantalate niobate substrate. Interfaces synthesized under high-temperature and high-oxygen-pressure conditions exhibit metallic conduction. Remarkably, well-defined metallic 2DEGs exhibiting pronounced hysteresis behavior and persistent electric-field-modulated resistance are observed below 108 K, with a resistance modulation of 11.6% at 7 K. These findings highlight the potential for extending these phenomena to other oxide-based 2DEG systems and motivate further investigation of ferroelectric metals in complex oxide heterostructures.

Keywords: oxide interfaces, two-dimensional electron gas (2DEG), $KTa_{1-x}Nb_xO_3$, ferroelectric modulation

PACS: 73.40.–c, 77.80.–e

DOI: 10.1088/1674-1056/ae5475 **CSTR:** 32038.14.CPB.ae5475

1. Introduction

Exploring and designing high-performance functional materials, such as high-entropy alloys, perovskite oxides, and topological materials, has become a key pathway in condensed matter physics for uncovering new states of matter and achieving technological breakthroughs.[1–4] The discovery of two-dimensional electron gases (2DEGs) at complex oxide interfaces has emerged as a prominent topic in condensed matter physics. Since the initial report by Hwang and coworkers on $LaAlO_3/SrTiO_3$ heterostructures,[5] extensive research has uncovered a spectrum of intriguing properties, such as giant persistent photoconductivity,[6] two-dimensional superconductivity,[7,8] interfacial ferroelectricity,[9] magnetism,[10] Rashba spin–orbit coupling (SOC),[11] and unique quantum transport behaviors.[12] Although most studies have focused on $SrTiO_3$-based systems — including $CaZrO_3/SrTiO_3$,[13] $BiFeO_3/SrTiO_3$,[14] $GdAlO_3/SrTiO_3$,[15] and $PrAlO_3/SrTiO_3$,[16] — recent efforts have extended the exploration of 2DEGs to other oxide materials. Notably, Zou *et al.*[17] reported a 2DEG at the $LaTiO_3/KTaO_3$ interface in 2015, and Zhang *et al.*[18] demonstrated a high-mobility 2DEG at an amorphous $LAO/KTaO_3$ interface in 2017. $KTaO_3$-based 2DEGs have attracted considerable attention due to their strong spin–orbit coupling (approximately 20 times greater than that of $SrTiO_3$[19,20]) — along with exceptional characteristics such as higher superconducting transition temperatures.[21–24] Recent studies have further advanced the understanding of oxide heterostructures. For example, Zhao *et al.*[25] observed a light-induced spin-polarized 2DEG with giant Rashba splitting at the $EuTiO_3/KTaO_3$ (111) interface, enabling optical control of spin–orbit coupling. Cui *et al.*[26] investigated charge transfer at the $Ni_3InN/SrVO_3$ interface, revealing interfacial electronic reconstruction. Beyond oxides, Shao *et al.*[27] studied the effect of p-GaN thickness on 2D hole gases in GaN/AlGaN/GaN heterostructures, emphasizing the importance of layer design in nitride systems. These findings enrich the understanding of interfacial 2D carrier gases and guide the design of functional heterostructures with tailored properties.

It should be noted that recent studies on the (111)-oriented $LAO/KTaO_3$ interface have revealed the coexistence and coupling of ferroelectricity and interfacial superconductivity,[28,29] demonstrating the extraordinary ability of ferroelectric order to regulate the superconducting state. In contrast, the present study focuses on the nonsuperconducting normal metallic state, aiming to investigate the reversible and nonvolatile modulation of fundamental transport properties, such as resistance, in a 2DEG by ferroelectric polarization in ferroelectric oxide substrates. This approach provides a novel proof of concept for electronic devices based on the ferroelectric metal concept. Despite these advances, the coexistence of ferroelectricity and metallic conductivity at oxide interfaces remains a fundamental challenge, particularly for applications in integrated sensing, memory, and comput-

†Corresponding author. E-mail: jinkx@nwpu.edu.cn

© 2026 Chinese Physical Society and IOP Publishing Ltd. All rights, including for text and data mining, AI training, and similar technologies, are reserved.

ing systems. This difficulty stems primarily from the screening of long-range Coulomb interactions by mobile charge carriers, which typically suppresses ferroelectric order.[30] Previous attempts to achieve ferroelectric modulation of resistance — using ferroelectric overlayers such as $Pb(Zr_xTi_{1-x})O_3$ or $BaTiO_3$ on $LaAlO_3/SrTiO_3$ heterostructures — have demonstrated significant resistive switching.[31–35] More recently, $Sr_{0.99}Ca_{0.01}TiO_3$-based 2DEGs exhibiting gate-tunable transport and nonvolatile resistance states have renewed interest in ferroelectric metals.[36] However, the low Curie temperature ($\sim$ 35 K) of $Sr_{0.99}Ca_{0.01}TiO_3$ limits its practical applicability at elevated temperatures.

In this study, we employ single-crystal $KTa_{0.9}Nb_{0.1}O_3$ (KTN) — a ferroelectric oxide from the 5d transition-metal family — as a substrate to host a high-quality 2DEG via the deposition of amorphous $LaAlO_3$ (LAO) films. KTN undergoes a ferroelectric phase transition near its Curie temperature,[37–41] offering a promising platform for coupling ferroelectricity with electronic transport. We present the first direct evidence of coexisting ferroelectricity and reversible resistance modulation at LAO/KTN heterointerfaces, thereby establishing a pathway toward functional oxide devices operable beyond cryogenic temperatures.

2. Experimental methods

The 2DEGs were fabricated by depositing LAO films onto (001)-oriented KTN single-crystal substrates ($5 \times 5 \times 0.5$ mm^3) via pulsed laser deposition (PLD). A systematic investigation of the transport characteristics was conducted by varying the growth temperature (T_g) (300 °C, 450 °C, and 600 °C) and oxygen pressure $P(O_2)$ (8×10^{-4} Pa, 5×10^{-3} Pa, 5×10^{-2} Pa, 1 Pa, and 5 Pa), while maintaining a constant repetition rate (1 Hz) and fluence ($\sim$ 1.6 J·cm^{-2}) of the KrF excimer laser ($\lambda = 248$ nm). The varied fabrication conditions are listed in Table S1 (Supporting Information). The thickness of LAO in all samples is 7.7 nm. Additionally, the dielectric constant versus temperature curve is shown in Fig. S1 (Supporting Information), which reveals a sharp transition at the Curie temperature $T_c = 108$ K, above which ferroelectric polarization vanishes. Furthermore, the *P*–*E* hysteresis loops of the KTN substrate at 80 K are shown in Fig. S2 (Supporting Information), providing evidence of typical ferroelectric characteristics. The surface morphology was analyzed using atomic force microscopy (AFM; MFP-3D). Room-temperature structural characterization was performed via x-ray diffraction (XRD; Bruker D2). The interfacial microstructure and elemental distribution were examined using high-resolution transmission electron microscopy (HRTEM) and energy-dispersive spectroscopy (EDS) on an FEI Themis Z instrument. Electronic transport properties were measured in the van der Pauw configuration using a physical property measurement system (PPMS; CFMS-14T).

3. Experimental results

The experimental results highlight the distinctive properties of the LAO/KTN heterointerface, underscoring its potential as a model system for ferroelectric 2DEGs.

AFM measurements show that the LAO film deposited at a T_g of 600 °C and an oxygen pressure $P(O_2)$ of 8×10^{-4} Pa has a root-mean-square roughness of approximately 244 pm (scan area: 1×1 μm^2), indicating good surface flatness that meets the basic requirements for preparing high-quality heterojunctions. Figure 1(b) shows a cross-sectional transmission electron microscopy image of the LAO/KTN heterojunction, clearly distinguishing the single-crystal KTN substrate, the interfacial region, and the upper amorphous LAO thin film. This image confirms the successful deposition of the film and the formation of the heterojunction. The XRD pattern of the sample (Fig. S3, Supporting Information) shows only Bragg reflections from the KTN substrate, confirming the amorphous nature of the LAO layer — a conclusion further supported by cross-sectional TEM imaging in Fig. 1(b). The interface is atomically sharp and flat, with the amorphous LAO (Area 1) situated directly atop the crystalline KTN substrate (Area 2). This structural contrast is further evidenced by FFT patterns: Area 1 shows a diffuse ring pattern without discernible diffraction spots, while Area 2 exhibits sharp lattice reflections. Figure 1(c) presents a high-angle annular dark-field scanning transmission electron microscopy (HAADF-STEM) image and corresponding EDS elemental maps across the LAO/KTN interface. All elements except Nb show clearly defined spatial distributions at the interface. To assess the dimensionality of electrical transport, out-of-plane and in-plane magnetoresistance measurements were performed (Fig. S4, Supporting Information). The observed magnetoresistance anisotropy confirms the two-dimensional nature of the conductive channel.

We systematically investigate the transport properties of LAO/KTN interfaces fabricated at varying T_g values while maintaining a fixed oxygen partial pressure of $P(O_2) = 8 \times 10^{-4}$ Pa. Figure 2(a) shows the temperature-dependent R_s for samples prepared at various T_g values. All samples exhibit metallic behavior, as indicated by a decrease in R_s with decreasing temperature. Notably, although the KTN substrate undergoes a paraelectric-ferroelectric phase transition near 108 K, no obvious anomalies appear in the in-plane resistance-temperature curves. First, the ferroelectric polarization is perpendicular to the interface and mainly modulates the confinement of the 2DEG by tuning the interfacial potential barrier, while in-plane transport is insensitive to such out-of-plane changes.[28] Second, the screening effect of the high-

density 2DEG may mask the phase-transition signal, as the high carrier density can partially compensate for the modulation caused by ferroelectric polarization.[42] The carrier density (n) as a function of temperature is presented in Fig. 2(b). For samples grown at $T_g = 300$ °C and 450 °C, n gradually decreases upon cooling, suggesting a higher density of defects in the 2DEGs formed at lower T_g values, which results in carrier freeze-out at low temperatures.[12] In contrast, the sample grown at $T_g = 600$ °C shows not only a reduced carrier density but also nearly temperature-independent behavior, indicating suppressed defect-mediated localization. Amorphous LAO thin films grown at lower temperatures may contain a higher concentration of structural defects, which act as carrier traps and lead to a decrease in effective carrier density upon cooling. In contrast, growth at 600 °C, with its higher deposition energy, promotes the formation of a denser amorphous structure with fewer defects. This suppresses trap-assisted carrier localization, resulting in an almost temperature-independent carrier density and higher mobility.

To further explore the role of the oxygen atmosphere during sample growth, we fixed T_g at 300 °C and varied the oxygen pressure during growth, including $P(O_2) = 8 \times 10^{-4}$ Pa, 5×10^{-3} Pa, 5×10^{-2} Pa, 1 Pa, and 5 Pa. The sample grown at 5 Pa was completely insulating (not shown). As shown in Fig. 2(d), the R_s–T behavior of the remaining samples consistently exhibits metallic conduction. The resistance does not decrease monotonically with oxygen partial pressure but instead reaches a minimum at a moderate oxygen pressure. This indicates a trade-off between carrier concentration and mobility: lower oxygen pressure increases carrier density via oxygen vacancies but introduces strong disorder scattering that sharply reduces mobility. Oxygen vacancies are critical to the formation of the 2DEG in KTN-based systems. When $P(O_2)$ is increased to 5×10^{-3} Pa, the carrier density (Fig. 2(e)) remains relatively stable across temperatures, suggesting suppressed charge localization. Further increases in $P(O_2)$ lead to a systematic reduction in n. Remarkably, the interface maintains metallic conduction even at $P(O_2) = 1$ Pa, exceeding the stability reported for LAO/KTO_3 heterointerfaces.[43] The temperature-dependent Hall mobility for all samples is summarized in Figs. 2(c) and 2(f). In all cases, the mobility increases with decreasing temperature. The highest mobility is observed in the sample grown at $T_g = 600$ °C, reaching ~ 98.0 $cm^2 \cdot V^{-1} \cdot s^{-1}$ at 7 K. Together, these results demonstrate that interfaces fabricated at high growth temperatures and high oxygen pressures exhibit optimal metallic characteristics, with reduced disorder and enhanced carrier mobility.

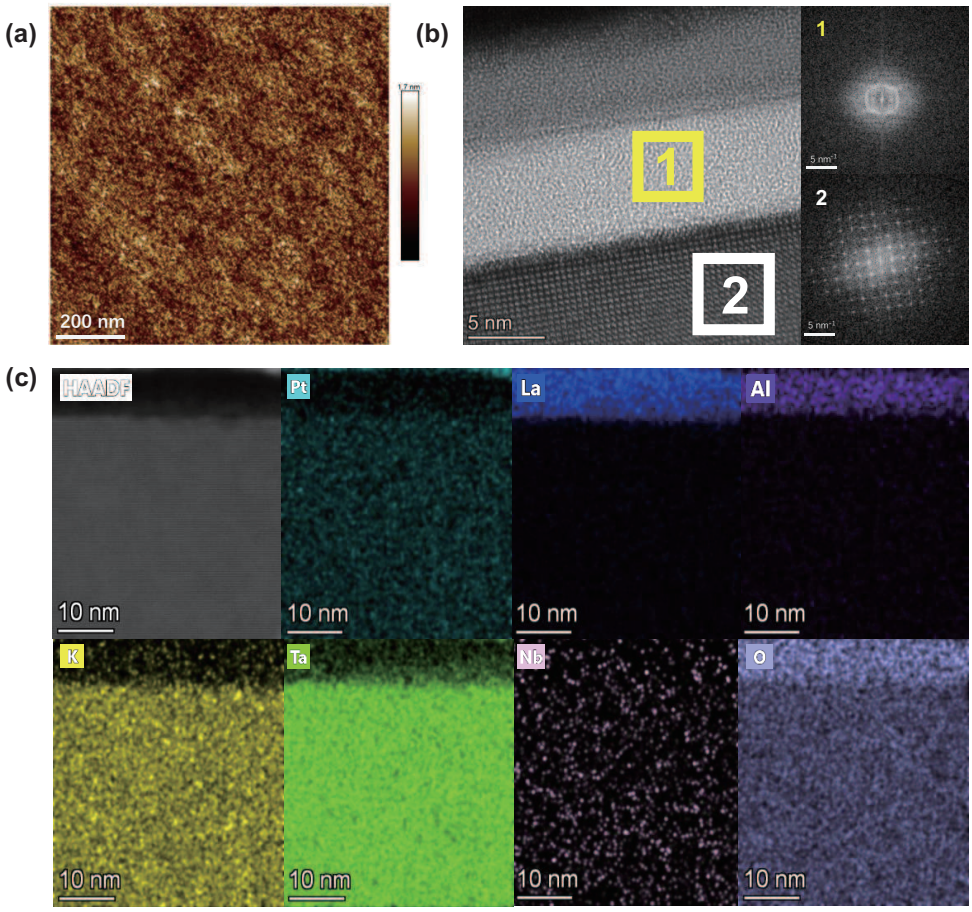

Fig. 1. (a) AFM image of the LAO film. (b) HRTEM images of the LAO/KTN interface. The insets show the FFT patterns of the corresponding regions. (c) HAADF image and EDS elemental maps near the interface.

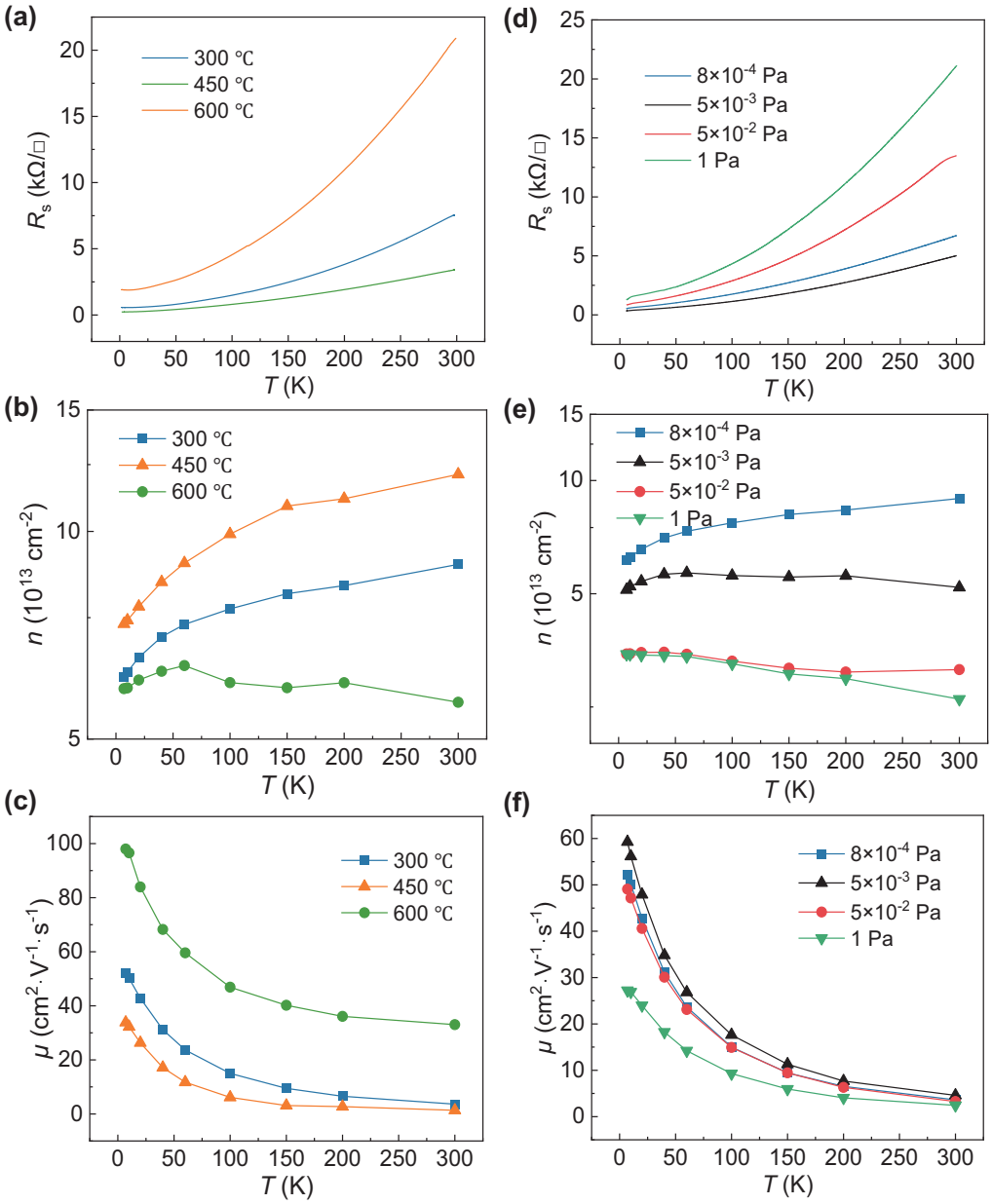

Fig. 2. Temperature dependence of the sheet resistance (a), carrier density (b), and carrier mobility (c) at a fixed oxygen pressure of $P(O_2) = 8 \times 10^{-4}$ Pa. Temperature dependence of the sheet resistance (d), carrier density (e), and carrier mobility (f) under different oxygen pressures at a fixed growth temperature of $T_g = 300$ °C.

Next, we investigated ferroelectric modulation of transport at the LAO/KTN interface grown at $T_g = 600$ °C and $P(O_2) = 8 \times 10^{-4}$ Pa. Figure 3(a) schematically illustrates the field-effect device. A top electrode is contacted to the LAO/KTN interface, and a silver back electrode is evaporated onto the rear side of the substrate, allowing a gate voltage perpendicular to the interface to be applied. Figure 3(b) presents the polarization-versus-vertical-electric-field loops for the sample. Clear *P*–*E* hysteresis confirms the ferroelectricity of the KTN substrate and shows pronounced ferroelectric switching. At 7 K, the polarization reaches its maximum value, and the loop displays a pronounced remanent polarization. As the temperature rises, the polarization decreases gradually; above 100 K, the *P*–*E* relationship becomes essentially linear, and the hysteresis disappears completely above the Curie temperature T_c.

To quantify the influence of ferroelectric polarization on 2DEG transport, we introduce the resistance-change ratio

$$\Delta R = (R(E) - R(0))/R(0) \times 100\%,$$

where $R(0)$ is the initial resistance without gate field and $R(E)$ is the resistance under field E. Figure 3(c) shows ΔR as a function of the applied electric field at various temperatures. Analogous to the *P*–*E* loops, when $T < T_c$, the KTN is in its ferroelectric single-domain state, and the ΔR–*E* curves exhibit pronounced hysteresis that becomes stronger upon cooling: the loops become fuller, and the maximum ΔR increases, reaching 11.6% at 7 K. At $T > T_c$, the hysteresis in the ΔR–*E* curves largely disappears.

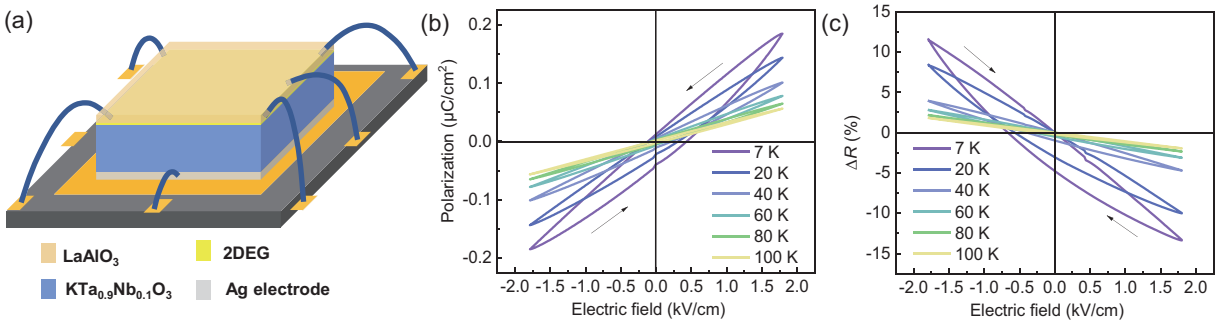

Fig. 3. (a) Schematic of the field-effect device based on the LAO/KTN heterointerface. (b) P–E hysteresis loops measured for the sample at different temperatures ($f = 1$ kHz). (c) The ΔR of the sample as a function of the applied electric field. The arrows indicate the directions of increasing and decreasing voltage.

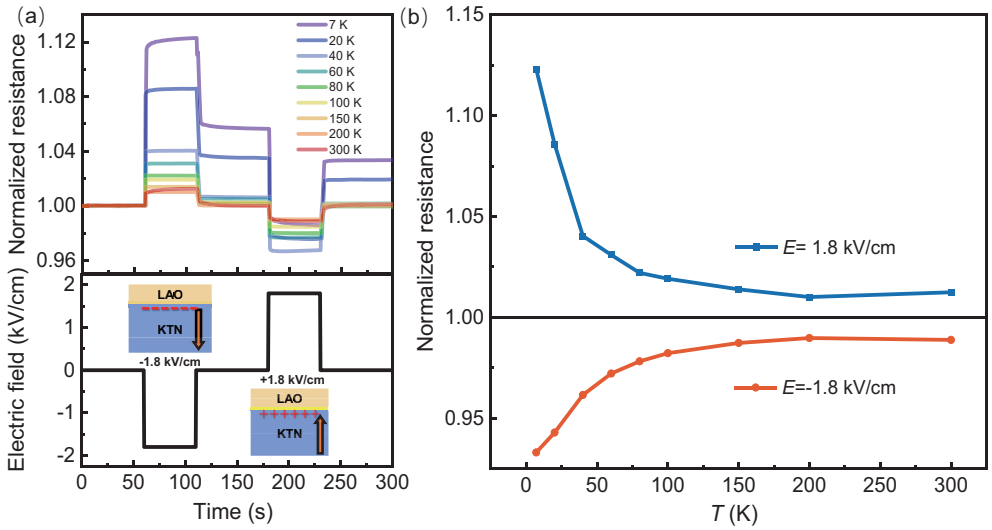

Fig. 4. (a) Time dependence of the normalized resistance of the LAO/KTN heterointerface at different temperatures when the electric field is switched between -1.8 and $+1.8$ kV/cm. The insets show the changes in polarization in the LAO/KTN heterointerface. (b) Normalized resistance of the LAO/KTN heterointerface as a function of temperature at -1.8 and $+1.8$ kV/cm (the stable resistance after applying the electric field relative to the resistance before applying the electric field).

We verify the ferroelectric origin of the observed hysteresis and rule out interfacial traps as the main contribution based on the following evidence. First, the highly nonvolatile resistance states are consistent with ferroelectric switching.[44] Second, the resistive hysteresis shows strong temperature dependence, becoming more pronounced at lower temperatures, consistent with enhanced ferroelectric switching at low temperatures. If the hysteresis originated from charge trapping, it would follow thermally activated behavior.[45] Furthermore, the gate-dependent resistive hysteresis in Fig. 3 resembles typical ferroelectric P–E loops, whereas charge trapping produces smoother and more linear hysteresis. These results indicate that ferroelectric polarization switching dominates the observed hysteresis.

Figure 4(a) illustrates the time dependence of the normalized resistance ($R/R(0)$) at different temperatures after applying electric fields of -1.8 kV/cm and $+1.8$ kV/cm. Initially, the sample was held at zero field for 60 s to establish a baseline. Subsequently, an electric field E alternating between -1.8 kV/cm and $+1.8$ kV/cm (corresponding to back-gate voltages of -90 V and $+90$ V, respectively) was applied, with each field maintained for 50 s, followed by a 70 s interval. Two remarkable features can be identified. First, the resistance at $E = -1.8$ kV/cm suddenly increases within milliseconds and then stabilizes at a nearly constant value. In contrast, the resistance at $E = +1.8$ kV/cm drops sharply due to upward polarization switching, confirming the tunability of the 2DEG. When a positive electric field is applied to the back gate, the resistance continues to decrease because the effect of ferroelectric polarization outweighs the increase in electron scattering under the applied gate voltage. This behavior can be understood as follows: the positive gate voltage induces ferroelectric polarization pointing toward the film, accumulating positive bound charges at the interface and attracting electrons, thereby increasing the 2DEG concentration. During this process, the carrier accumulation effect of ferroelectric polarization dominates over any possible enhancement of electron scattering under the gate field, leading to a continuous decrease in resistance. Conversely, a negative gate voltage induces polarization pointing toward the substrate, accumulating negative bound charges at the interface and depleting electrons. The depletion effect of ferroelectric polarization

dominates the transport behavior, resulting in an increase in resistance. Second, after the external electric field is removed, the resistance fully recovers to its initial state at temperatures above 108 K, where KTN is in the paraelectric phase, whereas it remains partially shifted at temperatures below 108 K, where KTN is in the ferroelectric phase. This behavior, illustrated in the inset of Fig. 4(a), is attributed to residual polarization at low temperatures. Figure 4(b) shows the temperature dependence of the normalized resistance, indicating that the normalized resistance approaches its initial value as the temperature increases. These results collectively demonstrate that the 2DEG at the LAO/KTN interface exhibits clear ferroelectric-coupled transport characteristics, including a kink in the resistance near T_c and hysteresis in R_s. Importantly, this system represents a pristine ferroelectric 2DEG, as the conducting channel is embedded directly within the ferroelectric host material KTN.

4. Conclusion

We have successfully realized a high-quality 2DEG with ferroelectric properties by depositing amorphous LAO films onto (001)-oriented ferroelectric KTN substrates. Our experimental results reveal that interfaces fabricated at elevated temperatures and under controlled oxygen pressure exhibit pronounced metallic characteristics, even though the LAO layer remains amorphous. Moreover, the 2DEG shows tunable transport properties and distinct resistance states under remanent polarization conditions. The resistance can be effectively modulated by sweeping the back-gate electric field, a response that closely mirrors the ferroelectric *P*–*E* hysteresis loop of the KTN substrate. These findings establish a promising approach for controlling interfacial charge transport through ferroelectric polarization, opening new pathways for exploring ferroelectric metals in complex oxide heterostructures and their potential applications in next-generation electronic devices.

Acknowledgments

Project supported by the National Natural Science Foundation of China (Grant Nos. 52373253 and 12374192) and the Natural Science Basic Research Program of Shaanxi (Grant Nos. 2025SYS-SYSZD-037 and 2025JC-YBQN-017).

References

[1] Wang H, Hu L, Xie W, Chang J, Zheng C, Li M, Wang Q, Liao H, Liu D and Wei B 2024 *Angew. Chem. Int. Ed.* **63** e202400312
[2] Zhao J F, Li M X, Wang H P and Wei B 2022 *Acta Mater.* **237** 118127
[3] Chow S L E, Luo Z and Ariando A 2025 *Nature* **642** 58
[4] Zheng D, Li Y, Liu C, Lan J, Jin C, Wang Q, Zhang L, Xi G, Fang B, Zhang C, Algaidi H, Chen A, Liu X, Yin G, Xu Z, Xiao J Q, Manchon A and Zhang X 2024 *Matter* **7** 3489
[5] Ohtomo A and Hwang H Y 2004 *Nature* **427** 423
[6] Eom K, Lee J, Yang G, Kim Y, Jeon J, Yeon J and Lee H 2023 *J. Mater. Sci. Technol.* **137** 152
[7] Herranz G, Singh G, Bergeal N, Jouan A, Lesueur J, Gázquez J, Varela M, Scigaj M, Dix N, Sánchez F and Fontcuberta J 2015 *Nat. Commun.* **6** 6028
[8] Singh G, Guzman R, Saïz G, Zhou W, Gazquez J, Masoudinia F, Winkler D, Claeson T, Fraxedas J, Bergeal N, Herranz G and Kalaboukhov A 2024 *Commun. Phys.* **7** 149
[9] Jang H W, Kumar A, Denev S, Biegalski M D, Maksymovych P, Bark C W, Nelson C T, Folkman C M, Baek S H, Balke N, Brooks C M, Tenne D A, Schlom D G, Chen L Q, Pan X Q, Kalinin S V, Gopalan V and Eom C B 2010 *Phys. Rev. Lett.* **104** 197601
[10] Li L, Richter C, Mannhart J and Ashoori R C 2011 *Nat. Phys.* **7** 762
[11] Lesne E, Saglam Y G, Battilomo R, Mercaldo M T, van Thiel T C, Filippozzi U, Noce C, Cuoco M, Steele G A, Ortix C and Caviglia A D 2023 *Nat. Mater.* **22** 576
[12] Briggeman M, Tomczyk M, Tian B, Lee H, Lee J, He Y, Tylan-Tyler A, Huang M, Eom C, Pekker D, Mong R S K, Irvin P and Levy J 2020 *Science* **367** 769
[13] Kwon D, Kwak Y, Lee D, Jo W, Cho B, Koo T and Song J 2023 *Sci. Rep.* **13** 15927
[14] Ji D, Zhang Y, Mao W, Gu M, Xiao Y, Yang Y, Guo W, Gu Z, Zhou J, Wang P, Nie Y and Pan X 2024 *APL Mater.* **12** 051103
[15] Li M, Dong H, Wei X, Yang R, Yin H, Wang S and Jin K 2021 *J. Phys. Chem. C* **126** 611
[16] Li M, Zhou Y, Chen Y, Yang R, Wei X, Wang S and Jin K 2021 *J. Phys. Chem. Lett.* **12** 1657
[17] Zou K, Ismail-Beigi S, Kisslinger K, Shen X, Su D, Walker F J and Ahn C H 2015 *APL Mater.* **3** 036104
[18] Zhang H Y, Yan X L, Zhang X, Zhang Q, Zhang J Y, Han F S, Gu L, Liu B, Chen Y Z, Shen B and Sun J L 2017 *ACS Appl. Mater. Interfaces* **9** 36456
[19] Uwe H, Sakudo T and Yamaguchi H 1985 *Jpn. J. Appl. Phys.* **24** 519
[20] Uwe H, Oka K, Unoki H and Sakudo T 1980 *J. Phys. Soc. Jpn.* **49** 577
[21] Zhang H Y, Yan X L, Zhang X, Wang S, Xiong C, Zhang H, Qi S, Zhang J Y, Han F S, Wu N, Liu B, Chen Y Z, Shen B and Sun J L 2019 *ACS Nano* **13** 609
[22] Liu C, Yan X, Jin D, Ma Y, Hsiao H, Lin Y, Bretz-Sullivan T M, Zhou X, Pearson J, Fisher B, Jiang J S, Han W, Zuo J, Wen J, Fong D D, Sun J, Zhou H and Bhattacharya A 2021 *Science* **371** 716
[23] Chen Z, Liu Y, Zhang H, Liu Z, Tian H, Sun Y, Zhang M, Zhou Y, Sun J and Xie Y 2021 *Science* **372** 721
[24] Chen X, Yu T, Liu Y, Sun Y, Lei M, Guo N, Fan Y, Sun X, Zhang M, Alarab F, Strocov V N, Wang Y, Zhou T, Liu X, Lu F, Liu W, Xie Y, Peng R, Xu H and Feng D 2024 *Nat. Commun.* **15** 7704
[25] Zhao Y C, Li J J, Wang Z, Zhou T L, Li M H, Shi W X, Hu F X, Sun J R, Li G, Chen Y Z and Shen B G 2026 *Chin. Phys. Lett.* **42** 100703
[26] Cui T, Zhou Y, Zhang Q H, Wang Q Y, Rong D K, Hong H T, Choi S, Xie A X, Zhang J J, Wang C, Ge C, Gu L, Wang S M, Jin K J, Dong S and Guo E J 2025 *Chin. Phys. Lett.* **42** 100705
[27] Shao P F, Cheng Y F, Liu Y, Yao Q, Qiao Z J, Peng Y H, Cai Q, Tao T, Xie Z L, Chen D J, Liu B, Zhang R and Wang K 2025 *Chin. Phys. B* **34** 117301
[28] Zhang M, Qin M, Sun Y, Hong S, Zhou Y and Xie Y 2025 *Nat. Commun.* **17** 219
[29] Dong M D, Cheng X B, Zhang M and Wu J 2026 *Nat. Commun.* (In press)
[30] Wang Y, Liu X, Burton J D, Jaswal S S and Tsymbal E Y 2012 *Phys. Rev. Lett.* **109** 247601
[31] Kim S, Kim D, Kim Y, Moon S Y, Kang M, Choi J K, Jang H W, Kim S K, Choi J, Yoon S, Chang H J, Kang C, Lee S, Hong S, Kim J and Baek S 2013 *Adv. Mater.* **25** 4612
[32] Tra V T, Chen J, Huang P, Huang B, Cao Y, Yeh C, Liu H, Eliseev E A, Morozovska A N, Lin J, Chen Y, Chu M, Chiu P, Chiu Y, Chen L, Wu C and Chu Y 2013 *Adv. Mater.* **25** 3357
[33] Wang S, Bai Y, Xie L, Li C, Key J D, Wu D, Wang P and Pan X 2018 *ACS Appl. Mater. Interfaces* **10** 1374
[34] Lee S R, Baasandorj L, Chang J W, Hwang I W, Kim J R, Kim J, Ko K, Shim S B, Choi M W, You M, Yang C, Kim J and Song J 2019 *Nano Lett.* **19** 2243
[35] Gao H, Peng W, Zhu X, Hu T, Xie X and Zhu J 2014 *Ceram. Int.* **40** 13763
[36] Bréhin J, Trier F, Vicente-Arche L M, Hemme P, Noël P, Cosset-Chéneau M, Attané J P, Vila L, Sander A, Gallais Y, Sacuto A, Dkhil B, Garcia V, Fusil S, Barthélémy A and Cazayous M 2020 *Phys. Rev. Mater.* **4** 041002

[37] Laguta V V, Glinchuk M D, Kuzian R O, Nokhrin S N, Bykov I P, Jastrabík L and Rosa J 2002 *Solid State Commun.* **122** 277
[38] Sakamoto T, Nakamura K, Fujiura K and Cho Y 2007 *Appl. Phys. Lett.* **90** 222908
[39] Yang Q, Li X, Liu H, Ren Y and Wu P 2021 *Chin. Opt. Lett.* **19** 111602
[40] Wu Y J, Liang F, Wang X, Wang J, Yu H F and Zhang H D 2022 *Opt. Mater. Express* **12** 247
[41] Wu Y J, Wang X, Tian G, Zheng L, Liang F, Zhang S, Yu H F and Zhang H D 2022 *Adv. Mater.* **34** 2105108
[42] Wang Y, Niranjan M K, Jaswal S S and Tsymbal E Y 2009 *Phys. Rev. B* **80** 165130
[43] Zhang H Y, Yan X L, Zhang J, Zhang J Y, Han F S, Huang H, Qi S, Shi W, Shen B and Sun J L 2019 *Mater. Res. Express* **6** 086448
[44] Kim J Y, Choi M J and Jang H W 2021 *APL Mater.* **9** 021102
[45] Fan Z, Fan H, Yang L, Li P L, Lu Z X, Tian G, Huang Z F, Li Z W, Yao J X, Luo Q Y, Chen C, Chen D Y, Yan Z B, Zeng M, Lu X B, Gao X S and Liu J M 2017 *J. Mater. Chem. C* **5** 7317